IEEE Access
Multidisciplinary | Rapid Review | Open Access Journal

Received May 3, 2017, accepted May 31, 2017, date of publication June 6, 2017, date of current version August 22, 2017.

Digital Object Identifier 10.1109/ACCESS.2017.2712659

Design and Analysis of a Reconfigurable Holographic Metasurface Aperture for Dynamic Focusing in the Fresnel Zone

OKAN YURDUSEVEN, (Senior Member, IEEE), DANIEL L. MARKS, JONAH N. GOLLUB, (Member, IEEE), AND DAVID R. SMITH, (Member, IEEE)

Center for Metamaterials and Integrated Plasmonics, Department of Electrical and Computer Engineering, Duke University, Durham, NC 27708, USA

Corresponding author: Okan Yurduseven (okanyurduseven@ieee.org)

This work was supported by the Air Force Office of Scientific Research under Grant FA9550-12-1-0491.

ABSTRACT We present numerical simulations of the near-field focusing capabilities of a dynamically reconfigurable holographic metasurface aperture. The aperture consists of a parallel-plate waveguide in which the upper plate is patterned with a number of metamaterial irises that can be dynamically switched between radiating (ON) and non-radiating (OFF) states. A cylindrically symmetric waveguide mode, excited by a coaxial probe in the center of the lower plate, serves to excite the radiating irises, forming a focused spot in the radiating near-field (or Fresnel zone). The layout of the metamaterial elements and their tuning states is determined using holographic design principles, in which the interference pattern of the waveguide (or reference) mode and the desired radiated field pattern leads to the required phase distribution over the surface of the aperture. We also develop an analytical model of the aperture to confirm the numerical simulations, and to illustrate the advantage of the guided-mode as the reference wave versus a plane-wave. We further leverage this analytical model to analyze the diffracted order characteristics of the holographic metasurface aperture, showing high-fidelity focusing patterns even for difficult focusing scenarios across the entire investigated field-of-view.

INDEX TERMS Near-field, focusing, reconfigurable, dynamic, metasurface, metamaterial, active, aperture, microwaves.

I. INTRODUCTION

Electronically reconfigurable apertures can dynamically control radiated phase-fronts without mechanical motion, enabling fast beam-forming. The ability to control the radiation phase-front of an aperture is of significant importance, giving rise to well-known capabilities within the distinctive radiation zones of the aperture; specifically, beam-focusing within the radiative near-field (Fresnel) region and beam-steering within the far-field (Fraunhofer) region.

Conventionally, most antennas are designed for far-field applications, including electronically scanned antennas (ESAs). Traditional ESAs rely on the distribution of a large array of antennas, each backed by an active phase-shifter, and which sample the aperture at the Nyquist limit ($\lambda/2$, where λ is the free-space wavelength) [1]–[6]. Such apertures have successfully been in use for decades for beam-forming and steering applications in the far-field, including radar and long-range communications. Although high-fidelity beam patterns have been demonstrated using phased array technologies, there are several limitations associated with these systems. For example, each antenna within a phased array aperture requires an individual phase shifting circuit, which, for even a moderately sized aperture, can result in a significant number of phase shifters. Thus, the active circuitry within the phase shifters forms a complex and expensive system architecture. Moreover, the phase shifters used in such systems exhibit considerable insertion losses, which must be offset using power amplifiers. Therefore, power consumption of such systems can be significant.

The concept of a metasurface to tailor the aperture radiated phase-fronts has successfully been demonstrated in the literature for near-field beam-focusing [7]–[9] and far-field beam-steering applications [9]–[11]. Metasurfaces consist of arrays of subwavelength elements whose electrical properties can be engineered to achieve desired electromagnetic responses. Numerous static metasurface designs across the electromagnetic spectrum have been reported in the literature and have shown great potential as alternative architectures for

wavefront shaping. The first dynamically reconfigurable metasurface was demonstrated in [12]–[16] at microwave frequencies (K-band, or 17.5 – 26.5 GHz), where far-field electronic beam scanning was achieved using a liquid-crystal layer whose dielectric constant could be varied in the vicinity of each metamaterial element using an externally applied voltage bias. By changing the local dielectric constant, the resonance frequency of each element within the metasurface aperture becomes voltage-controlled. Recently, the analysis of an electrically tunable liquid-crystal based metasurface layer has also been demonstrated [17]. While the liquid-crystal metasurface reconfigurable apertures exhibit high-fidelity beam control and can be integrated into large-scale manufacturing processes, liquid-crystal as a control mechanism imposes certain limitations, such as limited switching speed due to its inherent relaxation rate, typically on the order of up to 1 MHz. This limitation can be addressed by using semiconductor-based switching elements, such as PIN diodes, which exhibit switching speeds of up to a few GHz [18]. Such apertures were demonstrated in [16], [19], and [20] for far-field radar applications.

Using the concept of near-field focusing, many types of apertures have been demonstrated, including reflect arrays [21]–[23], transmit arrays [23]–[25] and Fresnel zone plates [23], [26]. Despite encouraging results, these structures require a non-planar feeding mechanism. Thus, they exhibit a poor form-factor, limiting their usage in applications where planar structures are desirable.

Other design alternatives that have recently become the subject of considerable research within the field of near-field focusing include microstrip arrays [27]–[33] and leaky-wave apertures [34]–[37]. Such apertures are conventionally planar and exhibit a small form-factor. However, a major drawback with most of these designs is that, similar to the static metasurface apertures discussed earlier, they are not reconfigurable and designed to achieve a fixed focus. Although the leaky-wave designs presented in [35]–[37] enable the control of the focusing depth within the near field as a function of the operating frequency, they do not offer the freedom to focus at an arbitrary point in space using the same aperture. The leaky-wave aperture presented in [34] exhibits reconfigurable operation achieved using field-effect transistors (FET). However, it can achieve dynamic beam-focusing only in one dimension due to the 1D geometry of the array aperture. Moreover, the guided mode is launched through a tapered horn antenna attached to a waveguide, resulting in a poor form-factor.

In this work, we demonstrate a reconfigurable, planar holographic metasurface aperture designed to achieve dynamic near-field beam-focusing in the Fresnel zone. While the reconfigurability enables the same aperture to be used to achieve varying focusing characteristics, the ability to dynamically focus the beam at any point within the near-field space of the aperture makes the proposed aperture suitable for a number of emerging applications, such as near-field imaging, non-destructive testing, biomedical imaging and wireless power transfer. The proposed aperture is based on a parallel-plate waveguide structure that operates at 20 GHz. The upper plate of the waveguide is populated with a set of metamaterial elements—simple rectangular irises, in the presented design, each of which can be toggled between radiating (ON) and non-radiating (OFF) states by switching a PIN diode, incorporated into the design, from reverse to forward bias. The distribution of radiating irises form a focus at some desired location determined using holographic design principles, as will be described below.

The outline of the paper is as follows: Section 2 explains the design of the dynamically reconfigurable holographic metasurface aperture for near-field focusing. In Section 3, we present simulated aperture radiated field-patterns for both on-axis and off-axis dynamic focusing scenarios. Analytical studies are also presented to analyze the focusing and diffracted order suppression limits of the presented aperture. The obtained results are analyzed and discussed. We provide concluding remarks in Section 4.

II. DYNAMICALLY RECONFIGURABLE HOLOGRAPHIC METASURFACE APERTURE

We illustrate the holographic aperture concept in Fig. 1, in which a dynamic aperture is shown producing a focused field at an arbitrarily selected point within the near-field of the aperture ($d < 2D^2/\lambda$, where D is the aperture size and λ is the free-space wavelength). As shown in Fig. 1, the aperture is center-fed using a coaxial cable inserted into the lower plate, with the upper plate discretized into a grid of elements, each subwavelength in dimensions. The reconfigurable aperture shown in Fig. 1 is a parallel-plate waveguide, consisting of a dielectric substrate, Rogers 3003 ($\varepsilon_r = 3$ and $\tan\delta = 0.001$), sandwiched between the top and bottom conducting layers. The size of the aperture is 15 cm $\times$ 15 cm, corresponding to an electrical size of $10\lambda \times 10\lambda$ at 20 GHz.

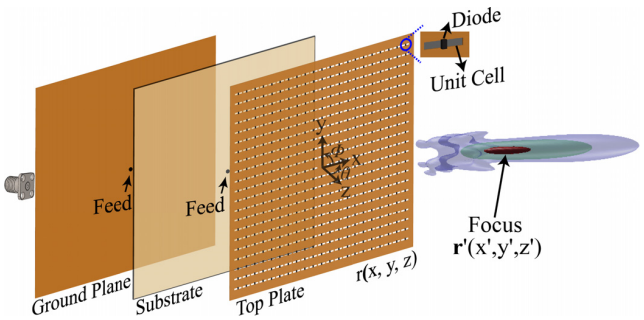

FIGURE 1. Structure of the reconfigurable aperture for focusing.

The magnetic field of the guided mode radiated by the coaxial feed into the dielectric substrate can be modeled by means of the Hankel function (zeroth order and first kind) as follows:

$$\mathbf{H}_{ref} = \begin{cases} H_0^1(k_g\mathbf{r})\cos\phi, & \text{x-polarization} \\ H_0^1(k_g\mathbf{r})\sin\phi, & y\text{-polarization} \end{cases} \quad (1)$$

In (1), k_g denotes the guided wavenumber ($k/\sqrt{\varepsilon_r}$) within the dielectric substrate and $\mathbf{r}$ is the position of the discretized

points on the aperture. For this analysis, it is assumed that the aperture is thin enough ($<\lambda_g/2$, where λ_g is the guided-wavelength within the dielectric substrate) along the optical axis (z-axis) to suppress the higher order waveguide modes (single mode operation) in the broadside direction. Following the definition of the guided-mode, the desired field distribution to create a focus at a selected point is calculated by treating the focused point as a fictitious point source placed at $\mathbf{r}'$ and back-propagating the radiated field from the point source to the aperture as follows:

$$\mathbf{P} = \frac{e^{-jk\left(\left|\mathbf{r}-\mathbf{r}'\right|\right)}}{\left|\mathbf{r}-\mathbf{r}'\right|} \tag{2}$$

Our aim is to produce a hologram over the metasurface aperture, such that the back-propagated field of (2) will be produced from the guided mode of (1), which can be considered the reference wave for the hologram. Analyzing (1) and (2), it is evident that this can be achieved from the complex amplitude distribution over the aperture surface (or mask) defined by

$$\mathbf{M} = \mathbf{P}\mathbf{H}_{ref}^{*} \tag{3}$$

In (3), $\mathbf{H}_{ref}^{*}$ denotes the complex conjugate of the guided magnetic field. In general, the phase dominates image formation, such that we attempt to reconstruct only the phase distribution implied by (3).

It should be noted that bold notation is adopted in (1)-(3) to represent vectors and matrices while we use scalar approximation for the fields. The elements used to form the metasurface (Fig. 1) resemble an array of slot antennas. It is well-known in antenna theory that a slot radiator has a resonance when the length of the slot is one-half the wavelength at the operating frequency [38]. Whereas such a choice ensures maximum coupling of the slots to the guided-mode (improving radiation efficiency), the strong coupling of the slot elements to the guided-mode can introduce a significant perturbation to the guided-mode (which is modeled here using the Hankel function as in (1) and ignoring scattering effects). With this tradeoff in mind, the length of the slot elements is taken to be slightly less than half of the guided-wavelength, $\lambda_g/2.5$, while the width of the slots is selected to be $\lambda_g/6$. The orientation of the elements governs the polarization of the radiation in three possible ways as depicted in Fig. 2.

A rectangular slot oriented along the x-axis will couple to the x-component of the guided magnetic field, therefore radiating a field linearly polarized along the x-direction [38]. Similarly, when oriented along the y-axis, the slots couple to the y-component of the magnetic field of the guided mode, radiating a field linearly polarized along the y-direction. When placed along the ϕ-direction, the slots couple both to the x- and y-components of the guided magnetic field, producing polarimetric radiation characteristics. These three possible states are depicted in Fig. 2. As shown in Fig. 1, the reconfigurable aperture presented in this work consists of slot unit cells oriented with their long axes along the x-axis, thus producing linearly polarized waves.

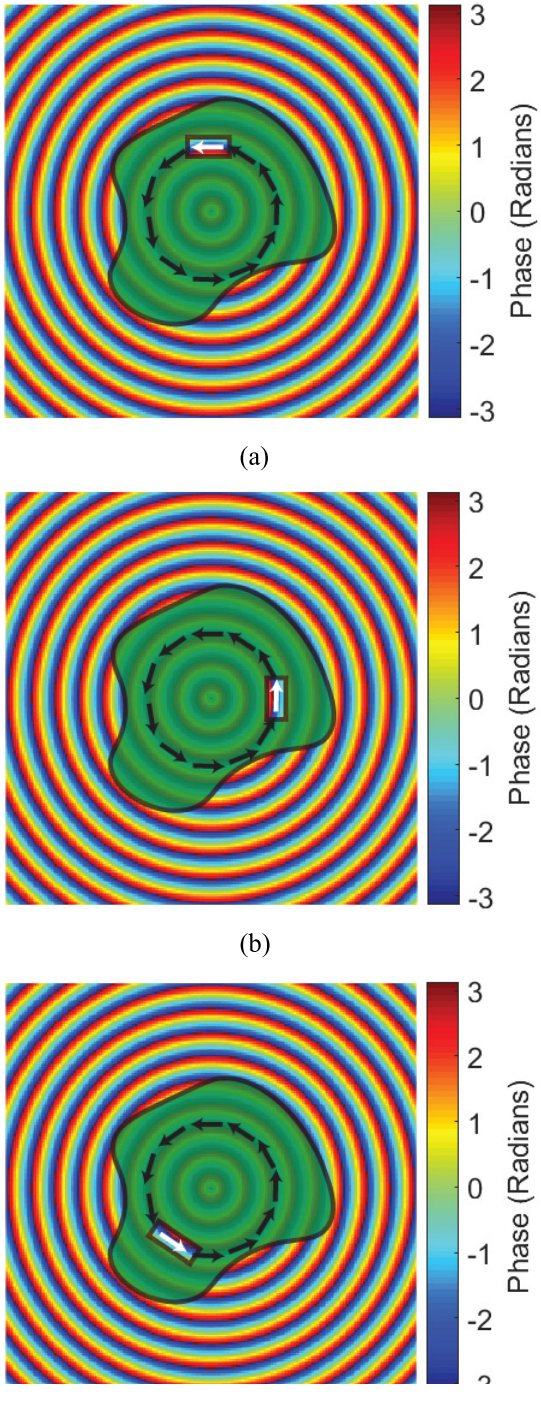

FIGURE 2. Orientation of the unit cells and coupling to the guided magnetic field (depicted as arrows): (a) horizontal (x-axis), (b) vertical (y-axis), and (c) ϕ-direction. The green layer depicts a portion of the conducting top layer of an arbitrary geometry onto which the metamaterial element, coupling to the guided mode, is patterned.

Each unit cell element patterned onto the front surface of the holographic metasurface aperture includes a PIN diode in the center, as depicted in Fig. 3(a), for which we assume

the circuit model of the PIN diode shown in Fig. 3(b). When forward-biased, the PIN diodes are modeled as an RL circuit with a negligible forward resistance in parallel with the junction capacitance, and an inductor in series as shown Fig. 3(b). When reverse-biased, the PIN diodes can be modeled as an LC circuit, exhibiting a high reverse resistance (effectively open-circuit), leaving the junction capacitance connected in series with the inductor.

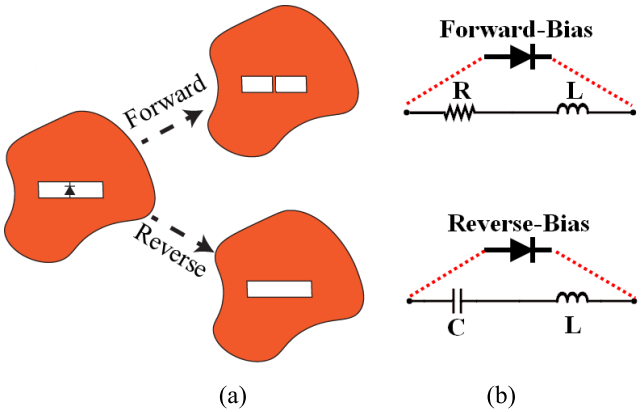

FIGURE 3. Unit cell loaded with a PIN diode (a) element configuration for forward and reverse bias states and (b) PIN diode equivalent circuit diagram; forward-biased: $R = 4\ \Omega$ and $L = 0.5$ nH, reverse-biased: $L = 5$ nH, $C = 0.02$ pF [18].

The PIN diodes are used to control the resonance frequency, and therefore the coupling response of the elements to the guided mode. As shown in Fig. 3(a), when forward-biased, the diodes short-circuit the slot unit cells (OFF state), shifting the resonance frequency of the slots to a higher frequency band. As a result, the OFF slots do not couple to the guided mode, acting as an opaque patch at the frequency band of interest. When reverse biased, the diodes act as an open-circuit element, enabling the slot unit cells to operate at the intended resonance frequency (ON state). To analyze the achievable contrast in the power level radiated by the OFF and ON unit cells, in CST Microwave Studio, we designed a parallel-plate waveguide consisting of a single slot unit cell patterned onto the front surface as shown in Fig. 4.

In Fig. 5, we show the simulated radiated power as a function of frequency of the metamaterial element when the PIN diode is forward- and reverse-biased, respectively. Both curves are normalized with respect to the maximum radiation and plotted on a logarithmic scale. Comparing the curves, it can be seen that at 20 GHz, the radiated power drops by a factor of 10 dB when the unit cell is OFF.

An important metric for the holographic metasurface aperture is the estimated power consumption. The number of metamaterial elements patterned onto the front surface of the aperture is 21×21. Given that each element includes a PIN diode, the aperture requires 441 PIN diodes. Biasing characteristic of conventional PIN diodes in the K-band are typically on the order of V=0.7 V and I=3 mA [18], resulting in the estimated power consumption per diode being equal to around 2.1 mW. Integrating over the full aperture,

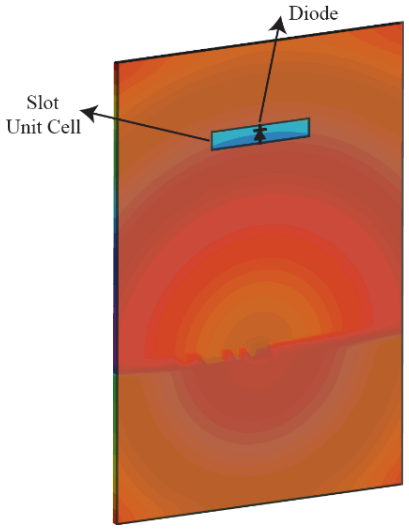

FIGURE 4. Parallel-plate waveguide with a single unit cell.

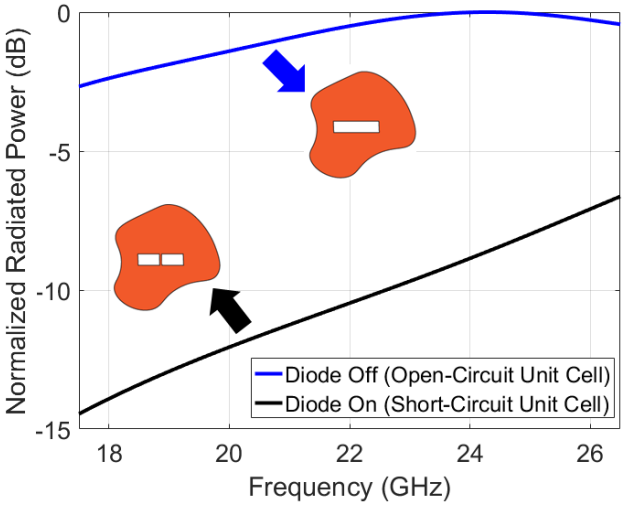

FIGURE 5. Single unit cell normalized radiated power patterns.

the estimated maximum power consumption is calculated to be 0.92 W, though it is unlikely that all elements will be activated at the same time. It should be noted that the practical implementation of the holographic metasurface aperture would require a DC biasing circuit to drive the PIN diodes. One potential solution would be to etch subwavelength-width lines (narrow enough to prevent any distortion to the guided-mode from an RF perspective) on the front layer of the aperture to accommodate the biasing circuit. Alternatively, a thin layer of dielectric laminate can be added to the design for DC biasing with metal vias connecting the biasing circuit to the diodes. Biasing of the diodes can be achieved using an Arduino driving an array of shift registers or a field-programmable gate array (FPGA) can be employed to achieve superior switching speed.

III. RESULTS AND DISCUSSION

To illustrate the dynamic beam focusing capability of the proposed reconfigurable holographic metasurface aperture, we choose two arbitrary points in space within the Fresnel

region of the aperture: F_1(x=0 m, y=0 m, z=0.5 m) and F_2(x=0 m, y=0.07 m, z=0.5 m) with F_1 and F_2 representing the on-axis and off-axis focusing points, respectively. For both scenarios, the aperture shown in Fig. 1 is used. It is known that the back-propagated aperture field distributions for these two focusing configurations will be different, suggesting that the patterns of the OFF and ON metamaterial elements within the aperture will be different for F_1 and F_2 focusing configurations.

We begin our analysis with the on-axis focusing scenario, F_1. Using (2), the calculated guided-mode within the parallel-plate waveguide is shown in Fig. 6(a). It should be noted that although the guided magnetic field within the parallel-plate waveguide exhibits a cylindrical wavefront comprising x- and y- components, because the slot elements on the aperture are oriented along the x-axis, we limit our attention to the x-component of the guided magnetic field as shown in Fig. 6(a). Fig. 6(b) demonstrates the phase pattern of the field radiated by the fictitious source F_1 back-propagated to the aperture plane.

Using (3), the calculated hologram mask, **M**, is presented in Fig. 6(c). The elements highlighted in white color are those with reverse-biased PIN diodes. These elements couple to the guided mode and contribute to the radiation (ON state). The elements highlighted in black color, on the other hand, are short-circuited with the forward-biased PIN diodes and thus do not couple to the guided mode—acting as opaque patches at the frequency band of interest (OFF state).

It should be noted that the phase advance introduced by the slot elements is negligible, which, when considering a particular point on the aperture, results in the phase of the field radiated by an element being approximately the same as the phase of the excited guided mode. As a result, in this work, we make use of a binary algorithm, relying on the principle of coupling only the elements positioned at the points where the phase difference between the guided mode, $\mathbf{H}_{ref}$, and the back-propagated pattern, **P**, remains within a certain threshold, which is selected to be $+/-20°$ as a result of numerical (CST Microwave Studio) parametric analyses. Therefore, the reconfigurable hologram mask in Fig. 6(c) can be considered a binary filter. Using more advanced unit cell topologies, such as complementary-ELC (cELC) and meander-line metamaterial elements [39], the phase accuracy and range of the hologram can be further increased.

Following the calculation of the hologram mask, the reconfigurable holographic metasurface aperture was designed in CST Microwave Studio. Fig. 7 illustrates the electric-field (E-field) pattern radiated by the aperture focusing at F_1(x=0 m, y=0 m, z=0.5 m). Fig. 7(a) shows the cross-section of the E-field pattern in the range plane (yz-plane), while Fig. 7(b) shows the E-field pattern at the focal plane (xy-plane at z=0.5 m). Observing the cross-range pattern in Fig. 7(b), it can be seen that the beam-waist is asymmetric due to the fact that the slot unit cells are narrower along one axis than the other. In order to analyze the focusing

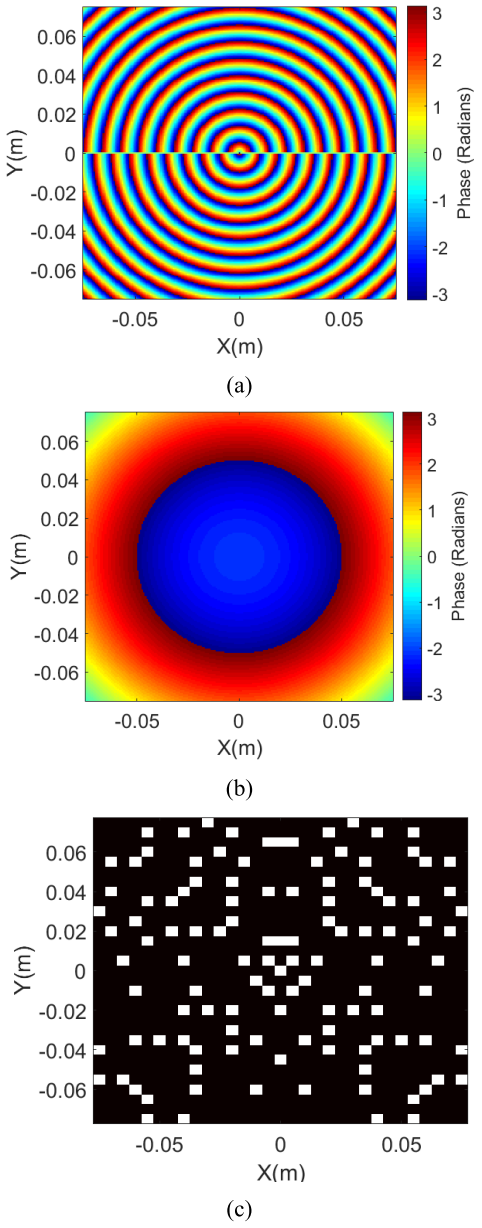

FIGURE 6. On-axis focusing: (a) guided-mode phase pattern, (b) back-propagated phase pattern on the aperture (from F_1), and (c) OFF (black) and ON (white) unit cell positions.

characteristics of the aperture, we investigate the -3dB full-width-half-maximum (FWHM) value of the beam-waist in the cross-range plane, which is found to be 4.9 cm (averaged along the x- and y-axes), suggesting good agreement with the theoretical limits calculated using the analytical equations presented in [40].

Following the on-axis scenario, we study off-axis focusing using the same reconfigurable aperture presented in Fig. 1. In comparison to the on-axis focusing scenario, for off-axis focusing, while the guided-mode shown in Fig. 6(a) remains the same (see Fig. 8(a)), the field back-propagated to the aperture from F_2 is different (see Fig. 8(b)), producing the hologram mask illustrated in Fig. 8(c) calculated using (3).

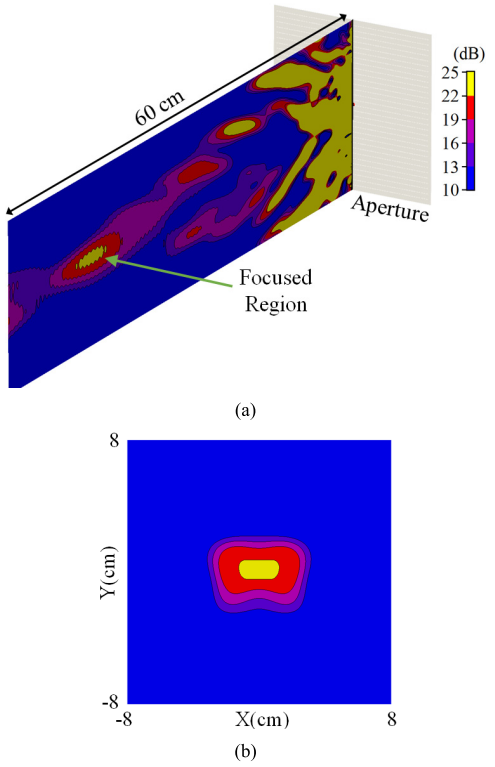

FIGURE 7. Radiated E-field pattern from the reconfigurable aperture: (a) range plane and (b) cross-range plane.

In Fig. 8(c), the elements highlighted in black are OFF due to the forward-biased diodes while the elements shown in white are ON and radiating. Similar to on-axis focusing, the phase threshold for the calculation of the hologram mask is selected to be $+/-20°$. The radiated E-field patterns in the range and cross-range planes are shown in Fig. 9.

Analyzing Fig. 9, the -3dB FWHM value for the beam-waist at the focal plane is found to be 5.2 cm. Comparing the FWHM values for the on-axis (Fig. 7) and off-axis (Fig. 9) scenarios, it is evident that the beam-waist for the off-axis configuration is wider than the on-axis configuration. This can be attributed to two factors; first, the focal distance of $|F_2|$, 0.505 m, is slightly larger than the focal distance of $|F_1|$, 0.5 m. Second, for the off-axis focusing scenario, the aperture is observed from an offset angle, $\theta \approx 10°$, resulting in a reduced effective aperture in comparison with the on-axis case. This widening factor in the beam-waist can be approximately predicted by dividing the on-axis beam by the factor $\cos^2\theta$ [40].

The choice of the reference-wave for the design of the reconfigurable metasurface aperture is of vital importance. In this work, we use the guided mode of (1), launched into the parallel-plate waveguide using the coaxial probe feed as depicted in Fig. 1. In holography, different types of waves can be used as the reference wave, including a plane-wave or a Gaussian beam [40]. An aperture using a plane-wave as the reference-wave can be considered to be the simplest type hologram from a computational perspective. However, using the proposed guided-mode in this work as the reference-wave

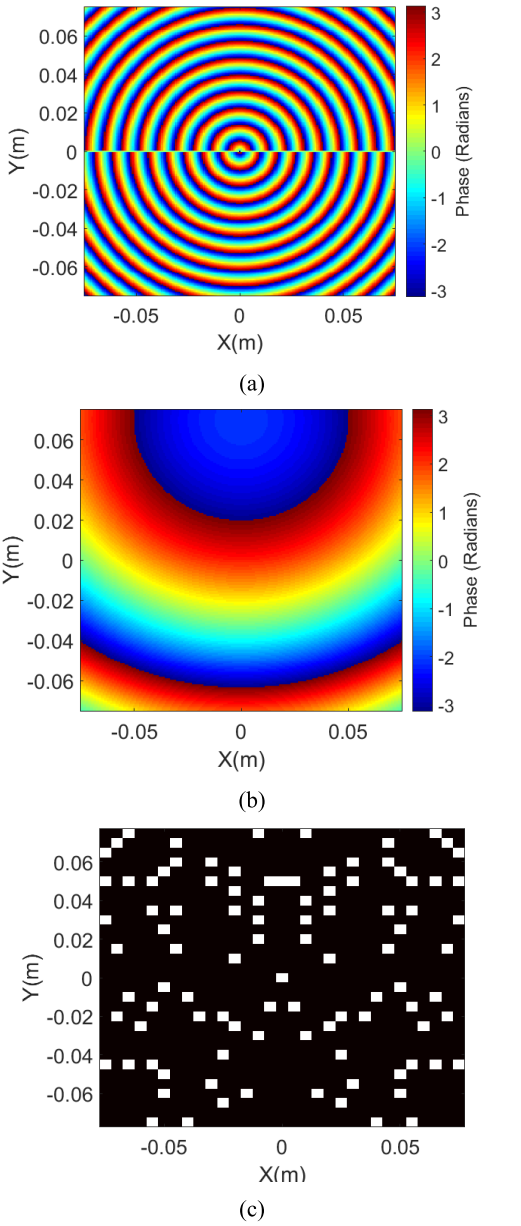

FIGURE 8. Off-axis focusing: (a) guided-mode phase pattern, (b) back-propagated phase pattern on the aperture (from F_2), and (c) OFF (black) and ON (white) unit cell positions.

brings significant advantages.

First, to have a plane-wave illuminating the aperture, the feeding source needs to be at a certain distance from the aperture to ensure that the aperture is illuminated with uniform phase-fronts. Such a feed naturally increases the overall profile of the composite structure, since the feed point must be at some significant distance from the aperture and may also require additional quasi-optical elements. The guided-mode launched by a simple, planar coaxial feed, by contrast, eliminates the need for focusing optics and offset sources, providing a significantly improved form factor.

Second, when a plane-wave is used to create the hologram, higher order diffraction modes are observed due to the limited phase-range of the hologram mask, which is selected to be

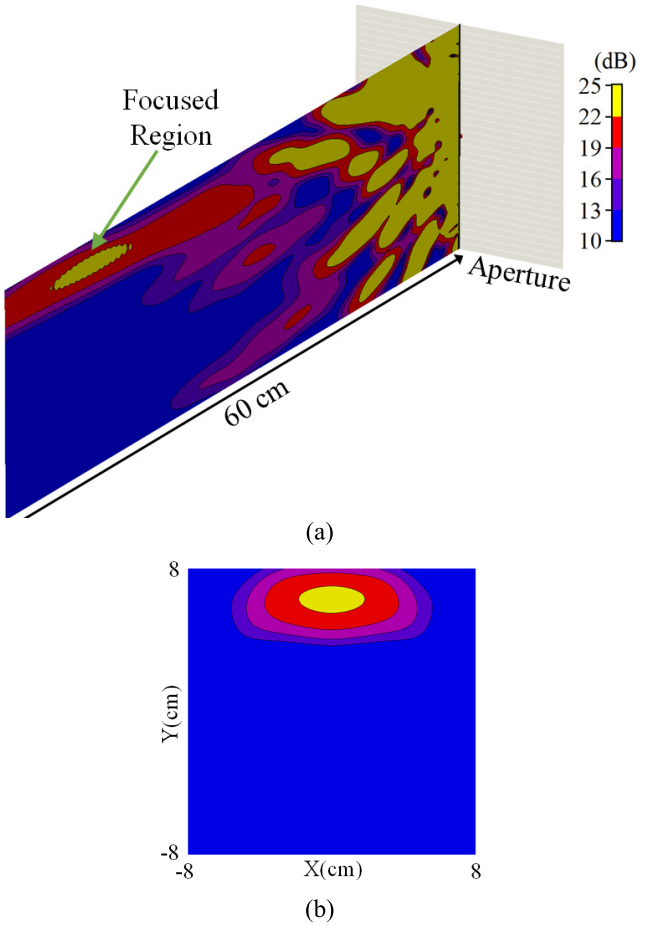

FIGURE 9. Radiated E-field pattern from the reconfigurable aperture: (a) range plane and (b) cross-range plane.

within the range of +/−20° in this work. This point can be illustrated using an analytical model of the reconfigurable metasurface aperture of Fig. 1, in which the slot elements are modeled as polarizable magnetic dipoles [41]. The radiation patterns can then be computed by summing the contributions of the dipoles, which we do using custom code written in Matlab. To compare with the guided wave reference, we also calculate the focusing characteristics of the holographic aperture designed using a plane-wave reference. For this study, the reference wave, $\mathbf{H}_{ref}$ in (1) is selected to be a plane-wave (uniform amplitude and phase) and the hologram mask is calculated using (3) for focusing at an arbitrarily selected point F_3 (x=0 m, y=0.3 m, z=0.5 m). The analytically calculated E-field pattern at the focal plane (z=0.5 m) is shown in Fig. 10.

Analyzing Fig. 10, it is evident that, in addition to the main focused beam (fundamental diffraction order – order 1 – of the aperture as highlighted in Fig. 10), higher order diffraction modes (order 0 and order −1) are present. These modes are undesirable because they reduce the amount of power delivered from the fundamental mode and can result in unwanted interference. The −3dB FWHM beam-waist of the focus is calculated to be 5.53 cm for the plane-wave reference scenario.

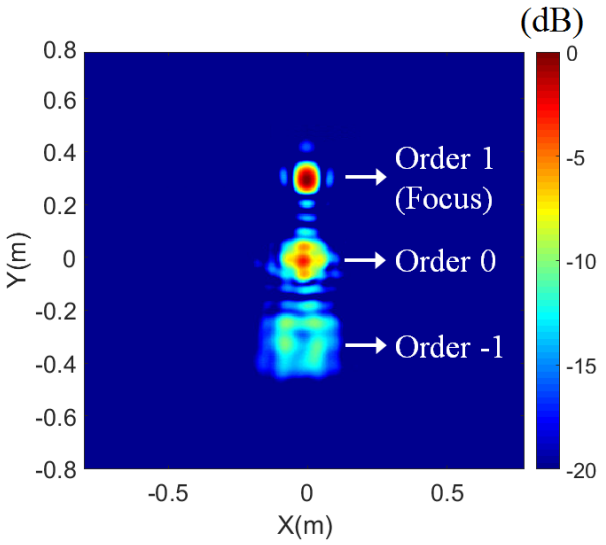

FIGURE 10. Analytical E-field pattern of the holographic aperture using plane-wave as the reference-wave. The aperture focusses at F_3 and the E-field pattern is demonstrated at the focal plane (z=0.5 m).

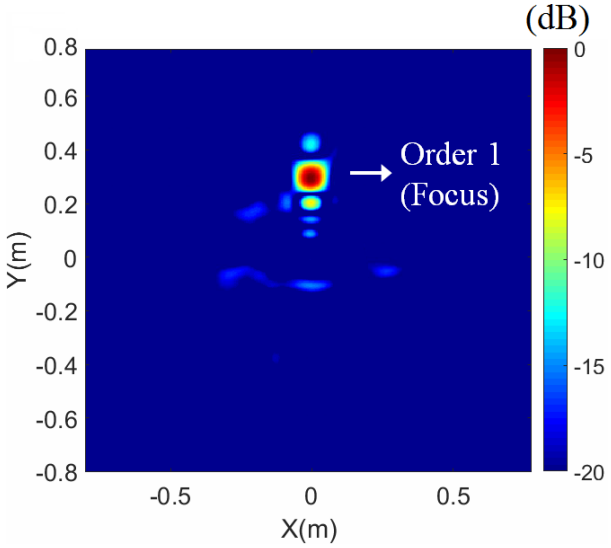

FIGURE 11. Analytical E-field pattern of the holographic aperture using the guided-mode of (1) as the reference-wave. The aperture focusses at F_3 and the E-field pattern is demonstrated at the focal plane (z=0.5 m).

With the cylindrical guided-mode of (1) taken as reference as shown in Figs. 6(a) and 8(a), the undesired higher order diffraction modes are suppressed. To provide the same comparison using the analytical model, we perform the same analytical study presented in Fig. 10, but replace the plane-wave reference with the guided-mode. The E-field pattern at the focal plane, z=0.5 m, is shown in Fig. 11.

Comparing Fig. 11 to Fig. 10, it is evident that when the guided mode is used as the reference wave, the higher order diffracted modes are suppressed, leaving only the main focusing beam. The -3dB beam-waist of the focus is calculated to be 6.3 cm, slightly larger than the beam-waist obtained using the plane-wave reference for the hologram, 5.6 cm. This can be attributed to the fact that while the plane-wave reference has a uniform amplitude, the amplitude of the guided-mode

of (1), which is a Hankel function, decays as a function of $1/\sqrt{r}$ in the transverse plane (xy-plane), where r denotes the distance from the center of the aperture. This suggests that the holographic metasurface aperture with the guided-mode reference exhibits an aperture amplitude tapering, widening the beam-waist of the focus. Another important conclusion from this study can be drawn by comparing the analytical and numerical beam-waist values of the holographic metasurface aperture with the guided-mode reference. Earlier, the numerical beam-waist for the on-axis scenario shown in Fig. 7 was calculated to be 4.9 cm. For the analytical study presented in Fig. 11, the offset angle is $\theta \approx 30°$. Using the $\cos^2\theta$ approximation presented in [40], the expected numerical beam-waist for the off-axis scenario demonstrated in Fig. 11 is 6.5 cm, exhibiting good agreement with the analytical beam-waist value, 6.3 cm.

Next, using the analytical model of the holographic reconfigurable metasurface aperture, we analyze the focusing and higher order mode suppression limits of the aperture. To this end, we sample a number of focusing locations as a function of θ and ϕ as depicted in Fig. 12. First, we choose four focusing points for $\theta = 45°$ and vary ϕ at 90° intervals. As a result, the studied focusing points are defined as follows:

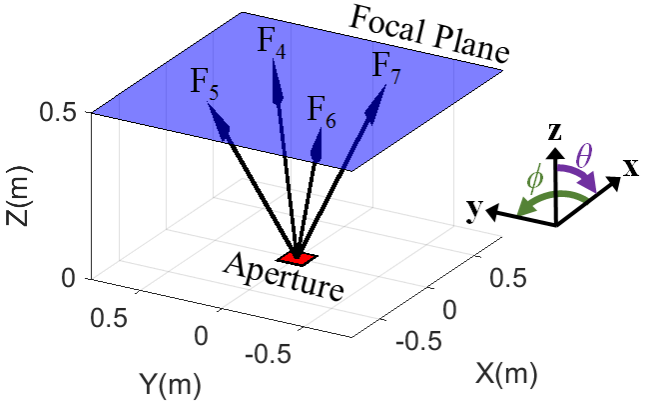

FIGURE 12. Depiction of the analyzed focusing locations (constant θ, varying ϕ).

- F_4(x=0.35 m, y=0.35 m, z=0.5 m) corresponding to (θ, ϕ)=(45°, 45°)
- F_5(x=−0.35 m, y=0.35 m, z=0.5 m) corresponding to (θ, ϕ)=(45°, 135°)
- F_6(x=−0.35 m, y=-0.35 m, z=0.5 m) corresponding to (θ, ϕ)=(45°, 225°)
- F_7(x=0.35 m, y=-0.35 m, z=0.5 m) corresponding to (θ, ϕ)=(45°, 315°)

The investigated focusing points for this study, F_4, F_5, F_6, and F_7, are depicted in Fig. 12.

In Fig. 13, the E-field patterns for focusing at F_4, F_5, F_6 an F_7 are shown at the focal plane, z=0.5 m.

Analyzing Fig, 13 reveals two important outcomes. First, focusing the beam at an offset angle widens the beam-waist of the focus, similar to the outcome observed in Fig. 9. Second, despite focusing at such extreme angles, the holographic

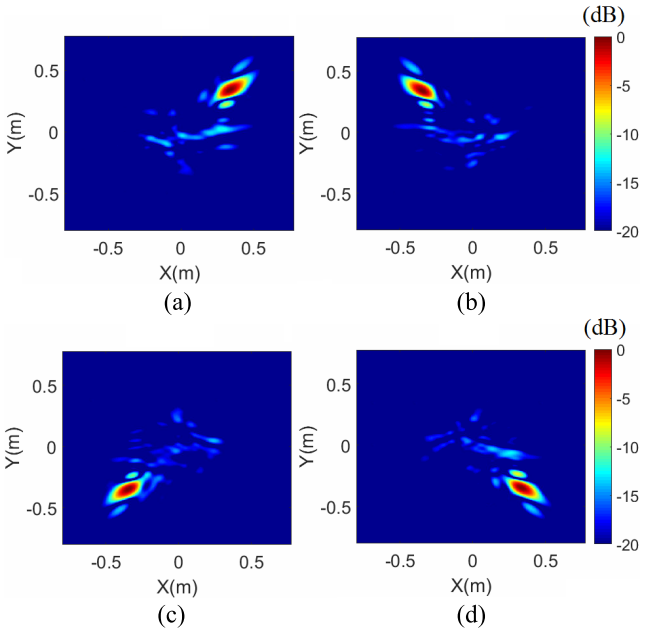

FIGURE 13. Calculated E-field patterns at the focal plane, z=0.5 m. Focusing at (a) F_4, (b) F_5, (c) F_6, and (d) F_7.

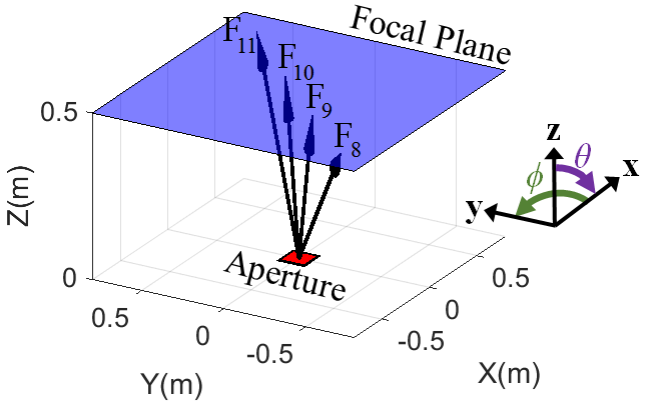

FIGURE 14. Depiction of the analyzed focusing locations (constant ϕ varying θ).

metasurface aperture successfully suppresses the higher diffraction orders, thanks to the guided-mode reference.

We next study the focusing characteristics and higher diffraction order suppression limits of the aperture as a function of constant ϕ (45°) and varying θ (from −60° to 60°). The sampled focusing points are as follows:

- F_8(x=−0.61 m, y =-0.61 m, z=0.5 m) corresponding to (θ, ϕ)=(−60°, 45°)
- F_9(x=−0.2 m, y =−0.2 m, z=0.5 m) corresponding to (θ, ϕ)=(−30°, 45°)
- F_{10}(x=0.2 m, y =0.2 m, z=0.5 m) corresponding to (θ, ϕ)=(30°, 45°)
- F_{11}(x=0.61 m, y =0.61 m, z=0.5 m) corresponding to (θ, ϕ)=(60°, 45°)

The investigated focusing points for this study, F_8, F_9, F_{10}, and F_{11}, are depicted in Fig. 14.

In Fig. 15, the E-field patterns for focusing at F_8, F_9, F_{10} an F_{11} are demonstrated at the focal plane, z=0.5 m.

Analyzing Figs. 15(a) and (d), it can be concluded that despite being almost 10 dB down in comparison to the ampli-

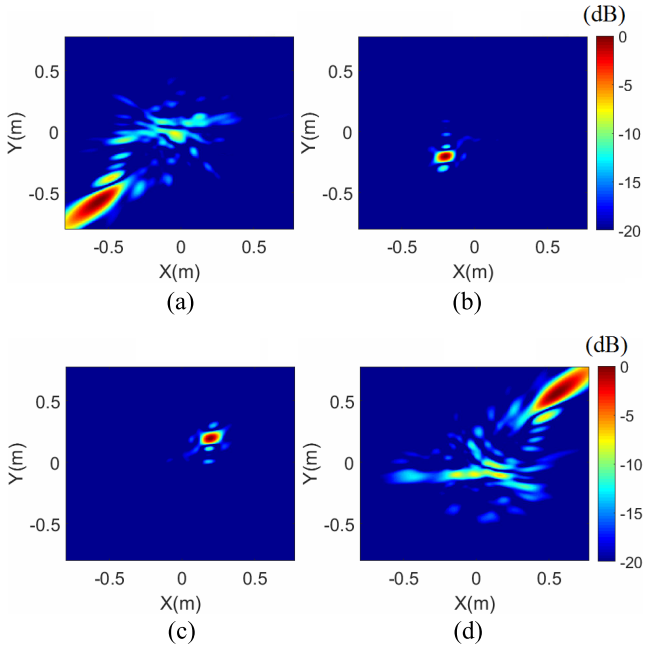

FIGURE 15. Calculated E-field patterns at the focal plane, z=0.5 m. Focusing at (a) F_8, (b) F_9, (c) F_{10}, and (d) F_{11}.

tude of the main focus, at focusing angles of θ=+/−60°, order 0 diffraction starts building along the optical axis of the aperture. For the focusing angles of θ=+/−30°, on the other hand, no unwanted diffraction orders are present and the focused beams exhibit good fidelity.

As mentioned earlier, when coupled to the guided-mode, the phase advance introduced by the slot unit cells is negligible. As a result, we activate (ON state) only the unit cells satisfying a certain phase threshold range between the guided-mode and the desired phase pattern on the aperture (back-propagated from the fictitious point source to be focused). As given earlier, this threshold range is selected to be +/−20°. Using more advanced unit cell topologies, one can design a holographic metasurface aperture, exhibiting full phase control. Such a design can convert the phase of the guided-mode to the desired phase pattern on the aperture for focusing, in theory, with 100% accuracy. As an example, using the developed analytical model, in Fig. 16, we analyze focusing at F_{11} (x=0.61 m, y=0.61 m, z=0.5 m) with full phase control.

Comparing Fig. 16 to Fig. 15(d), it is evident that the beam fidelity is improved and superior suppression in the order 0 diffraction region (along the broadside direction of the aperture) is achieved. This is an ongoing research effort and the results will be reported elsewhere.

IV. CONCLUSION

We have presented a reconfigurable holographic metasurface aperture for dynamic beam-focusing applications at 20 GHz. It has been shown that using an aperture consisting of an array of dynamically controlled elements, the phase-front of the aperture radiated fields can be reconfigured, enabling focusing of the aperture radiated fields at any point within the near-field in a dynamic manner. The studied numerical (CST Microwave Studio) and analytical results demonstrate the ability of the proposed holographic metasurface aperture to exhibit high-fidelity beam-focusing even when extreme focusing angles are considered. Although demonstrated for K-band frequencies, the developed aperture can readily be scaled to higher frequencies to achieve superior focusing resolution. The reconfigurable holographic metasurface aperture holds significant potential in several applications where having a dynamic control over near-field beams is desired, including near-field imaging [42]–[45], non-destructive testing, biomedical imaging and wireless power transfer [40].

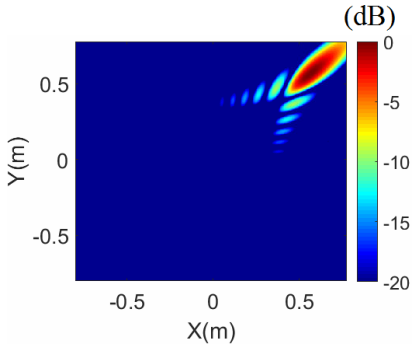

FIGURE 16. Calculated E-field pattern at the focal plane, z=0.5 m. Focusing at F_{11} with full phase control.

REFERENCES

[1] R. C. Hansen, *Phased Array Antennas*, 2nd ed. Hoboken, NJ, USA: Wiley, 2009.
[2] F. C. Williams and W. H. Kummer, "Electronically scanned antenna," U.S. Patent 4 276 551, Jun. 30, 1981.
[3] B.-H. Ku *et al.*, "A 77–81-GHz 16-element phased-array receiver with ±50o beam scanning for advanced automotive radars," *IEEE Trans. Microw. Theory Techn.*, vol. 62, no. 11, pp. 2823–2832, Nov. 2014.
[4] S. Withington, G. Saklatvala, and M. P. Hobson, "Partially coherent analysis of imaging and interferometric phased arrays: Noise, correlations, and fluctuations," *J. Opt. Soc. Amer. A, Opt. Image Sci.*, vol. 23, no. 6, pp. 1340–1348, 2006.
[5] G. L. Charvat, L. C. Kempel, E. J. Rothwell, C. M. Coleman, and E. L. Mokole, "An ultrawideband (UWB) switched-antenna-array radar imaging system," in *Proc. IEEE Int. Symp. Phased Array Syst. Technol.*, Oct. 2010, pp. 543–550.
[6] A. J. Fenn, D. H. Temme, W. P. Delaney, and W. E. Courtney, "The development of phased array radar technology," *Lincoln Lab. J.*, vol. 12, no. 2, pp. 321–340, 2000.
[7] M. Ettorre *et al.*, "On the near-field shaping and focusing capability of a radial line slot array," *IEEE Trans. Antennas Propag.*, vol. 62, no. 4, pp. 1991–1999, Apr. 2014.
[8] M. Ettorre, S. C. Pavone, M. Casaletti, and M. Albani, "Experimental validation of Bessel beam generation using an inward Hankel aperture distribution," *IEEE Trans. Antennas Propag.*, vol. 63, no. 6, pp. 2539–2544, Jun. 2015.
[9] A. Ludwig, J. P. S. Wong, A. Epstein, A. M. H. Wong, G. V. Eleftheriades, and C. D. Sarris, "Focusing and steering for medical applications with magnetic near-field arrays and metasurfaces," in *Proc. 9th Eur. Conf. Antennas Propag. (EuCAP)*, Lisbon, Portugal, 2015, pp. 1–4.
[10] A. Epstein and G. V. Eleftheriades, "Passive lossless Huygens metasurfaces for conversion of arbitrary source field to directive radiation," *IEEE Trans. Antennas Propag.*, vol. 62, no. 11, pp. 5680–5695, Nov. 2014.
[11] B. Ratni, A. de Lustrac, G.-P. Piau, and S. N. Burokur, "Design of nonuniform metasurfaces for beam steering performances," in *Proc. 10th Eur. Conf. Antennas Propag.*, Davos, Switzerland, 2016, pp. 1–4.
[12] N. Kundtz, "Next generation communications for next generation satellites," *Microw. J.*, vol. 57, no. 8, pp. 56–64, 2014.

[13] M. C. Johnson, S. L. Brunton, N. B. Kundtz, and J. N. Kutz, "Sidelobe canceling for reconfigurable holographic metamaterial antenna," *IEEE Trans. Antennas Propag.*, vol. 63, no. 4, pp. 1881–1886, Apr. 2015.
[14] R. Stevenson, M. Sazegar, A. Bily, M. Johnson, and N. Kundtz, "Metamaterial surface antenna technology: Commercialization through diffractive metamaterials and liquid crystal display manufacturing," in *Proc. 10th Int. Congr. Adv. Electromagn. Mater. Microw. Opt. (METAMATERIALS)*, 2016, pp. 349–351.
[15] Kymeta Corporation, accessed on Apr. 21, 2017. *mTenna*. [Online]. Available: http://www.kymetacorp.com/products/
[16] E. Brookner, "Metamaterial advances for radar and communications," *Microw. J.*, vol. 59, no. 11, pp. 22–42, 2016.
[17] S. C. Pavone, E. Martini, F. Caminita, M. Albani, and S. Maci, "Surface wave dispersion for a tunable grounded liquid crystal substrate without and with metasurface on top," *IEEE Trans. Antennas Propag.*, vol. 65, no. 7, pp. 3540–3548, Jul. 2017.
[18] *MACOM MA4AGBL912 PIN Diode*, accessed on Apr. 21, 2017. [Online]. Available: https://cdn.macom.com/datasheets/MA4AGBLP912.pdf
[19] PARC. *Metamaterial Devices and Applications*, accessed on Apr. 21, 2017. [Online]. Available: https://www.parc.com/services/focus-area/metamaterials/
[20] Echodyne Corporation. *MESA*, accessed on Apr. 21, 2017. [Online]. Available: http://echodyne.com/technology
[21] H.-T. Chou, T.-M. Hung, N.-N. Wang, H.-H. Chou, C. Tung, and P. Nepa, "Design of a near-field focused reflectarray antenna for 2.4 GHz RFID reader applications," *IEEE Trans. Antennas Propag.*, vol. 59, no. 3, pp. 1013–1018, Mar. 2011.
[22] H.-T. Chou, P.-H. Hsueh, T.-M. Hung, L.-R. Kuo, and H.-H. Chou, "A dual-band near-field focused reflectarray antenna for RFID applications at 0.9 and 2.4 GHz," *Radio Sci.*, vol. 46, no. 6, 2011, Art. no. RS6010.
[23] P. Nepa, A. Buffi, A. Michel, and G. Manara, "Technologies for near-field focused microwave antennas," *Int. J. Antennas Propag.*, Mar. 2017, Art. no. 7694281.
[24] E. G. Plaza, G. León, S. Loredo, and F. Las-Heras, "Near-field focusing transmitarray lens," in *Proc. 9th Eur. Conf. Antennas Propag.*, 2015, pp. 1–5.
[25] H. A. E.-A. Malhat, S. Zainud-Deen, and W. Hassan, "Different designs of dual-focus perforated transmitarray antenna in near/far-field region," *Adv. Electromagn.*, vol. 4, no. 3, pp. 25–34, 2015.
[26] S. Karimkashi and A. A. Kishk, "Focusing properties of Fresnel zone plate lens antennas in the near-field region," *IEEE Trans. Antennas Propag.*, vol. 59, no. 5, pp. 1481–1487, May 2011.
[27] A. Buffi, A. A. Serra, P. Nepa, H.-T. Chou, and G. Manara, "A focused planar microstrip array for 2.4 GHz RFID readers," *IEEE Trans. Antennas Propag.*, vol. 58, no. 5, pp. 1536–1544, May 2010.
[28] R. Siragusa, P. Lemaitre-Auger, and S. Tedjini, "Tunable near-field focused circular phase-array antenna for 5.8-GHz RFID applications," *IEEE Antennas Wireless Propag. Lett.*, vol. 10, pp. 33–36, 2011.
[29] F. Tofigh, J. Nourinia, M. Azarmanesh, and K. M. Khazaei, "Near-field focused array microstrip planar antenna for medical applications," *IEEE Antennas Wireless Propag. Lett.*, vol. 13, pp. 951–954, 2014.
[30] M. Bogosanovic and A. G. Williamson, "Microstrip antenna array with a beam focused in the near-field zone for application in noncontact microwave industrial inspection," *IEEE Trans. Instrum. Meas.*, vol. 56, no. 6, pp. 2186–2195, Dec. 2007.
[31] K. D. Stephan, J. B. Mead, D. M. Pozar, L. Wang, and J. A. Pearce, "A near field focused microstrip array for a radiometric temperature sensor," *IEEE Trans. Antennas Propag.*, vol. 55, no. 4, pp. 1199–1203, Apr. 2007.
[32] L. Shan and W. Geyi, "Optimal design of focused antenna arrays," *IEEE Trans. Antennas Propag.*, vol. 62, no. 11, pp. 5565–5571, Nov. 2014.
[33] V. R. Gowda, O. Yurduseven, G. Lipworth, T. Zupan, M. S. Reynolds, and D. R. Smith, "Wireless power transfer in the radiative near field," *IEEE Antennas Wireless Propag. Lett.*, vol. 15, pp. 1865–1868, 2016.
[34] Y. Monnai and H. Shinoda, "Focus-scanning leaky-wave antenna with electronically pattern-tunable scatterers," *IEEE Trans. Antennas Propag.*, vol. 59, no. 6, pp. 2070–2077, Jun. 2011.
[35] A. J. Martinez-Ros, J. L. Gómez-Tornero, F. J. Clemente-Fernandez, and J. Monzó-Cabrera, "Microwave near-field focusing properties of width-tapered microstrip leaky-wave antenna," *IEEE Trans. Antennas Propag.*, vol. 61, no. 6, pp. 2981–2990, Jun. 2013.
[36] J. L. Gómez-Tornero, D. Blanco, E. Rajo-Iglesias, and N. Llombart, "Holographic surface leaky-wave lenses with circularly-polarized focused near-fields—Part I: Concept, design and analysis theory," *IEEE Trans. Antennas Propag.*, vol. 61, no. 7, pp. 3475–3485, Jul. 2013.
[37] D. Blanco, J. L. Gómez-Tornero, E. Rajo-Iglesias, and N. Llombart, "Holographic surface leaky-wave lenses with circularly-polarized focused near-fields—Part II: Experiments and description of frequency steering of focal length," *IEEE Trans. Antennas Propag.*, vol. 61, no. 7, pp. 3486–3494, Jul. 2013.
[38] C. A. Balanis, *Antenna Theory: Analysis and Design*, 3rd ed. Hoboken, NJ, USA: Wiley, 2005.
[39] G. Lipworth, N. W. Caira, S. Larouche, and D. R. Smith, "Phase and magnitude constrained metasurface holography at W-band frequencies," *Opt. Exp.*, vol. 24, no. 17, pp. 19372–19387, 2016.
[40] D. R. Smith *et al.*, "An Analysis of beamed wireless power transfer in the Fresnel zone using a dynamic, metasurface aperture," *J. Appl. Phys.*, vol. 121, no. 1, p. 014901, 2017.
[41] G. Lipworth *et al.*, "Metamaterial apertures for coherent computational imaging on the physical layer," *J. Opt. Soc. Amer. A, Opt. Image Sci.*, vol. 30, no. 8, pp. 1603–1612, 2013.
[42] O. Yurduseven, V. R. Gowda, J. N. Gollub, and D. R. Smith, "Printed aperiodic cavity for computational and microwave imaging," *IEEE Microw. Wireless Compon. Lett.*, vol. 26, no. 5, pp. 367–369, May 2016.
[43] O. Yurduseven, J. N. Gollub, A. Rose, D. L. Marks, and D. R. Smith, "Design and simulation of a frequency-diverse aperture for imaging of human-scale targets," *IEEE Access*, vol. 4, pp. 5436–5451, 2016.
[44] D. L. Marks, O. Yurduseven, and D. R. Smith, "Cavity-backed metasurface antennas and their application to frequency diversity imaging," *J. Opt. Soc. Amer. A, Opt. Image Sci.*, vol. 34, no. 4, pp. 472–480, 2017.
[45] O. Yurduseven, V. R. Gowda, J. N. Gollub, and D. R. Smith, "Multistatic microwave imaging with arrays of planar cavities," *IET Microw., Antennas Propag.*, vol. 10, no. 11, pp. 1174–1181, 2016.

OKAN YURDUSEVEN (S'09–M'11–SM'16) received the B.Sc. and M.Sc. degrees in electrical engineering from Yildiz Technical University, Istanbul, Turkey, in 2009 and 2011, respectively, and the Ph.D. degree in electrical engineering from Northumbria University, Newcastle upon Tyne, U.K., in 2014.

From 2009 to 2011, he was a Research Assistant with the Department of Electrical and Electronic Engineering, Marmara University, Istanbul, Turkey. From 2011 to 2014, he was a Lecturer (part-time) with the Faculty of Engineering and Environment, Northumbria University. Since 2014, he has been a Post-Doctoral Associate with the Center for Metamaterials and Integrated Plasmonics, Department of Electrical and Computer Engineering, Duke University. His current research seeks to develop coded metasurface apertures for microwave and millimeter-wave computational imaging applications in collaboration with the U.S. Department of Homeland Security.

He has authored over 70 technical journal and conference publications, and three provisional patents. His current research interests include microwave and millimeter-wave imaging, multiple-input-multiple-output radar, wireless power transfer, antennas and propagation, antenna measurement techniques, and metamaterials. He has organized and chaired several special sessions within these fields in various international conferences, including the IEEE International Symposium on Antennas and Propagation and European Conference on Antennas and Propagation.

Dr. Yurduseven was a recipient of the Academic Excellence Award from the Association of British–Turkish Academics in London in 2013. He also received the Best Paper Award at the Mediterranean Microwave Symposium in 2012 and a travel grant from the Institution of Engineering and Technology (IET). He recently received the Duke Post-Doctoral Professional Development Award and has been nominated for the Outstanding Post-Doctoral Award at Duke University. He is a member of the European Association on Antennas and Propagation. He serves as a reviewer for several journals, including the IEEE TRANSACTIONS ON ANTENNAS AND PROPAGATION, the IEEE TRANSACTIONS ON MICROWAVE THEORY AND TECHNIQUES, the IEEE ANTENNAS AND WIRELESS PROPAGATION LETTERS, and *Progress in Electromagnetics Research*, and *Applied Physics B*.

DANIEL L. MARKS was born in Chicago, Illinois, in 1973. He received the B.S., M.S., and Ph.D. degrees from the University of Illinois at Urbana-Champaign in 1995, 1998, and 2001. From 2002 to 2008, he was a Research Scientist with the Biophotonics Laboratory, University of Illinois at Urbana-Champaign. He is currently an Associate Research Professor with the Department of Electrical and Computer Engineering, Duke University, which he joined in 2009. He has authored 85 research articles, 17 patents, and has been an Editor of Applied Optics. His current research interests include optics, optical design, computational imaging, millimeter-wave and terahertz imaging, metamaterials, and synthetic electromagnetic structures.

His research theme is the joint design of sensing systems with corresponding computational methods.

While at the University of Illinois, he was a Co-Inventor of Interferometric Synthetic Aperture Microscopy, a method of applying synthetic aperture radar reconstruction methods to 3-D biological imaging and nonlinear interferometric vibrational imaging, a method of high resolution Raman spectroscopy using femtosecond radiation.

He was the Lead Optical Designer of the DARPA AWARE Wide FOV Project, where he designed the optics for cameras varying from 0.3 to 8.5 gigapixels, as well as designed and implemented GPU-based real-time gigapixel-scale stitching algorithms. He also designed a super-broadband and compact short and long wave infrared weapon scope for the DARPA Dual Use Detector Ensemble Project. He is currently a member of the Duke Center for Metamaterials and Integrated Plasmonics Metamaterial Millimeter-Wave Imager project, for which he develops antennas, algorithms, and GPU computational methods.

JONAH N. GOLLUB (M'16) received the B.A. degree in physics from Reed College in 2000, and the Ph.D. degree in physics from the University of California at San Diego, San Diego, in 2009. His thesis work involved characterizing the hybridization of metamaterials with magnetic materials. From 2010 to 2012, he was a Lead Modeling and Simulation Scientist with a startup company developing surface metamaterials with applications targeted toward imaging and biological detection under DARPA, MDA, Army, and NSF funded efforts. He joined Duke University as a Research Scientist in 2013. He is currently focused on developing real-time millimeter wave imaging approaches which utilize frequency diverse antennas and compressive imaging techniques.

DAVID R. SMITH (M'98) is currently the Department Chair and James B. Duke Professor of electrical and computer engineering with Duke University and the Director of the Center for Metamaterials and Integrated Plasmonics. He also holds the adjunct professor positions with the Physics Department, University of California at San Diego; is an affiliate faculty with the Electrical and Computer Engineering Department, University of Washington; and a visiting professor of physics with Imperial College, London. He received the Ph.D. degree in physics from the University of California at San Diego (UCSD), San Diego, in 1994. His research interests include the theory, simulation and characterization of unique electromagnetic structures, including photonic crystals and metamaterials, as well as applications of such materials.

While at UCSD, he and his colleagues demonstrated the first left-handed (or negative index) metamaterial at microwave frequencies in 2000. He has more than 300 publications on matematerials and plasmonics. He was selected by ISI-Reuters as a Citation Laureate in 2009 for the most number of highly cited papers in the field of physics over the last decade. He was once again recognized as one of the Highly Cited Researches 2014 by ISI-Reuters in the category of Physics.

In 2002, Dr. Smith was elected a member of The Electromagnetics Academy. In 2005, he was part of a five member team that received the Descartes Research Prize, awarded by the European Union, for their contributions to metamaterials and other novel electromagnetic materials. He also received the Stansell Research Award from the Pratt School of Engineering, Duke University in 2005. In 2006, he was selected as one of the Scientific American 50, a group recognized by the editors of *Scientific American* for achievements in science, technology and policy. His work has twice appeared on the cover of *Physics Today,* and twice has been selected as one of the Top Ten Breakthroughs of the year by *Science Magazine.* In 2013, he was a co-recipient of the James C. McGroddy Prize for New Materials, received by the American Physical Society.

In 2006, he, along with colleague Sir John Pendry, suggested metamaterials could be used to design an electromagnetic cloak, introducing the new design tool of transformation optics. In 2013, he was asked to write an op-ed piece for the *New York Times* on cloaking research.

In 2013, he served as the Founding and Acting Director of the Metamaterials Commercialization Center (MCC), a unit within the Intellectual Ventures (Bellevue, WA) dedicated to commercializing metamaterials concepts. MCC has thus far produced three spin out companies: Kymeta Corporation (Redmond, WA), Evolv Technologies (Waltham, MA), and Echodyne (Bellevue, WA). He serves on the Advisory Board for Kymeta, which targets metamaterial-based antennas for satellite communications, and is a Co-Founder of Evolv Technologies, which targets metamaterial apertures for security screening applications, as well as Echodyne, which is seeking to apply metamaterial apertures to radar applications.